Original article

A NMR investigation of spontaneous and forced imbibition of shale under different flow and confinement conditions

Lingli Zheng[1], Jiahao Jiang[1], Wenlian Xiao[1], Bingqian Zhu[2], Yves Bernabé[3], Junqiang Zhang[4]

[1]*State Key Laboratory of Oil and Gas Reservoir Geology and Exploitation, Southwest Petroleum University, Chengdu 610500, P. R. China*
[2]*Research Institute of Petroleum Exploration & Development, CNPC, Beijing 100083, P. R. China*
[3]*Earth, Atmospheric and Planetary Sciences Department, Massachusetts Institute of Technology, Cambridge 02139, USA*
[4]*Sinopec Southwest Petroleum Bureau Downhole Service Co., SINOPEC, Deyang 618300, P. R. China*

Abstract:
In the development of shale gas reservoirs, hydraulic fracturing is followed by an imbibition (or soaking) stage, during which the fracturing wetting fluid migrates into the reservoir matrix. As a consequence, laboratory imbibition experiments have been performed in shale samples. However, these tests were generally conducted at atmospheric pressure and thus only involved spontaneous imbibition, which does not correspond to *in-situ* reservoir conditions. This study addresses this limitation by conducting forced imbibition experiments in shale samples at different flow and confinement conditions while measuring the nuclear magnetic resonance T_2 relaxation spectra at regularly increasing times. It was observed that increasing the initial pressure difference between the upstream and downstream ends of the sample (hereafter called the differential pressure) significantly improved gas displacement efficiency by promoting greater water migration into the shale pore space. Moreover, it was found that decreasing the confinement (i.e., by lowering the effective pressure) further enhanced the imbibition displacement efficiency, which reaches a maximum when the effective pressure approaches zero and spontaneous imbibition occurs. Reducing the effective pressure leaded to a substantial increase in the water intake and the formation of micro-cracks, as confirmed by post-mortem scanning electron microscopy images. These results emphasize that the differential pressure and effective pressure are key factors influencing the imbibition efficiency and the related microstructural changes in shale rocks. The study highlights the importance of replicating *in-situ* pressure conditions in future research and provides valuable insights for optimizing gas recovery strategies in shale gas reservoirs.

1. Introduction

Shale gas, predominantly found in organic-rich shale reservoirs, has emerged as a critical resource for the global energy supply (Hughes, 2013; Kerschke and Schulz, 2013). However, the inherent low porosity and permeability of shale reservoirs present considerable challenges for efficient gas extraction. To overcome these barriers, hydraulic fracturing has been widely implemented for stimulating shale reservoirs (Testamanti and Rezaee, 2017; Yu et al., 2023). The hydro-fracturing process causes extension of pre-existing natural fractures as well as the formation of secondary fractures, thus creating a complex interconnected fracture network. This three-dimensional network substantially enhances reservoir connectivity, enabling fluid

migration and significantly expanding the production area. Moreover, hydraulic fracturing operations generally use water-based wetting fluids that tend to penetrate the shale formation by imbibition.

Imbibition refers to the displacement within the porous medium of non-wetting fluids (e.g., gas) by wetting fluids (e.g., water). In shale reservoirs, imbibition plays a pivotal role in fluid transport, fracture filling, and pressure balance, making it a key factor for optimizing gas recovery. Despite its importance, past studies primarily focussed on spontaneous imbibition under atmospheric pressure conditions, thus failing to accurately reflect the high fluid pressures present *in-situ*. Makhanov et al. (2012) experimentally analyzed the effects of various base fluid types, polymer-enhanced viscosity, salinity, and other factors on the spontaneous imbibition of shale. Li et al. (2013) explained the influence of S_w on spontaneous imbibition based on the existing foundation and combined with fluid mechanics. Akbarabadi and Piri (2014) conducted a study on nanotomography of the spontaneous imbibition in shale. Rezaveisi et al. (2012) and You et al. (2019) investigated water saturation and imbibition characteristics under atmospheric conditions, concluding that water absorption is strongly influenced by imbibition area and wettability. Similarly, Ali et al. (2020) and Saidzade et al. (2020) examined shale wettability and porosity during imbibition, while Cai et al. (2014) and Ding et al. (2021) developed theoretical models to characterize imbibition behavior. Lu et al. (2022) investigated the capillary imbibition phenomenon and its mechanisms of shale oil in nanochannels. Recent studies (Pan et al., 2022; Zhao et al., 2023) emphasize the significant impact of chemical osmosis and confining pressures on shale imbibition behavior, demonstrating substantial differences in imbibition under realistic reservoir conditions. Although these studies provide valuable insights into the mechanics of imbibition, they largely neglect the influence of *in-situ* reservoir conditions, such as high fluid pressure gradients and significant overburden stresses, which are critical for understanding imbibition under realistic conditions.

Moreover, traditional methods for measuring imbibition, such as the weighing method, often lack precision due to the small volumes of fluid imbibed in tight samples (Wang et al., 2015; Ali et al., 2020; Yuan et al., 2023). To address these limitations, Nuclear Magnetic Resonance (NMR) has emerged as a powerful analytical tool for quantifying imbibition behavior with high accuracy (Yang et al., 2018; Yuan et al., 2023). NMR enables non-destructive, real-time monitoring of fluid distribution within the rock pore space, providing detailed insights into the dynamics of fluid migration. Studies using NMR have identified distinct T_2 relaxation spectra for fluid types, pore connectivity, and saturation levels in shale samples (Lai et al., 2016; Liu et al., 2018; Cheng et al., 2021; Sun et al., 2022; Su et al., 2022; Wei et al., 2023; Du et al., 2024). For instance, Gao and Li (2015) and Sun et al. (2016) emonstrated that NMR can differentiate between bound water and movable fluid in tight reservoirs, while Wang et al. (2020) revealed that imbibition efficiency correlates positively with experimental pressure. Wei et al. (2024) quantitatively analyzed the microscopic production characteristics and dynamic development patterns of shale oil during the processes of imbibition and huff-n-puff injection using online NMR technology. Dou et al. (2024) investigated the impact of imbibition on fluid migration, oil recovery enhancement, and the evolution of rock physical properties during massive energy replenishment in tight oil reservoirs by utilizing NMR technology. Wang et al. (2024) utilized LF-NMR technology to explore effective methods for enhancing oil recovery through imbibition flooding experiments. These findings highlight NMR's unique ability to analyze imbibition mechanisms under various conditions. The previous researches on imbibition characteristics of shales mainly rely on spontaneous imbibition experiment under atmospheric condition, which is not consistent with the actual condition of the formation (Roychaudhuri et al., 2013; Siddiqui et al., 2019; Tang et al., 2024). However, a systematic investigation of how differential and effective pressures affect imbibition in shale reservoirs remains underexplored.

To bridge these gaps, this study investigates the influence of differential pressure and effective pressure on shale imbibition behavior under reservoir-like conditions. Two experimental schemes were designed using shale samples collected from the Sichuan Basin, a region with significant shale gas reserves: (1) Imbibition experiments under different differential pressures and (2) imbibition experiments under different effective pressures. These tests were specifically designed to examine fluid migration and micro-crack development during imbibition. Our aim was to monitor imbibition dynamics by recording the T_2 relaxation spectra and pore fluid content during imbibition tests under controlled pressure conditions. Additionally, Scanning Electron Microscopy (SEM) was used to analyze microstructural changes, such as crack formation and pore network expansion, caused by imbibition. This study provides a comprehensive understanding of the interplay between differential and effective pressures and their impact on the displacement efficiency of imbibition in shale samples. The findings offer theoretical insights and practical guidance for optimizing gas recovery strategies in shale gas reservoirs.

2. Experimental section

2.1 Materials

Two shale samples (labeled S1 and S2) were obtained from the Sichuan Basin, a region with high-quality shale gas reserves. These samples were selected to provide a comparative analysis of imbibition behavior under varying pressure conditions. The properties of these two shale samples are summarized in Table 1. To replicate the ionic environment of reservoir fluids while minimizing clay swelling and chemical alteration, a 50,000 ppm potassium chloride (KCl) solution was used as the experimental fluid.

2.2 Experiments

This study employed a systematic experimental approach to investigate imbibition dynamics under distinct differential pressure and effective pressure conditions, using the NMR technology. The experimental objectives were: (1) Differential pressure effects: To evaluate the impact of differential pressure on fluid migration and gas-water displacement efficiency. (2)

Table 1. Properties of shale samples.

Samples	Dry weight (g)	Diameter (cm)	Length (cm)	Density (g/cm^3)	Porosity (%)	Permeability (mD)
S1	75.58	2.537	5.779	2.588	7.480	0.021
S2	70.56	2.539	5.431	2.574	4.360	0.012
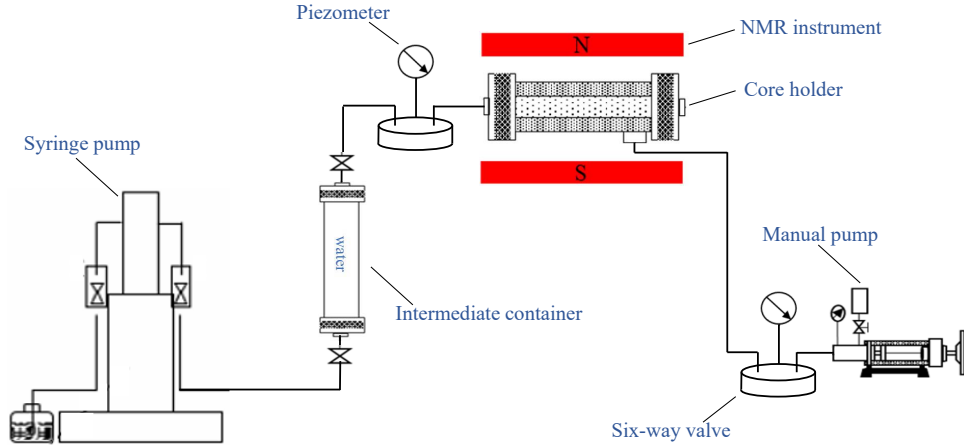
Fig. 1. Flow chart of shale pressure imbibition experiment.

Effective pressure effects: To assess the role of effective pressure in modifying pore connectivity, microfracture development, and fluid imbibition behavior. NMR technology was chosen for its non-destructive, high-resolution capabilities, enabling precise, real-time tracking of fluid migration and distribution within the pore structure of shale. This approach ensured accurate characterization of imbibition mechanisms under reservoir-like conditions.

2.2.1 Experimental setup

The experimental apparatus (schematic shown in Fig. 1) consisted of three main components.

(1) Core holder with integrated NMR instrumentation

The transition of the hydrogen nucleus from an unbalanced state to an equilibrium state is referred to as the relaxation process, which can be categorized into transverse relaxation and longitudinal relaxation. The transverse relaxation time is directly proportional to pore size, making it a valuable parameter for characterizing fluid distribution within pores. Additionally, the area enclosed by the T_2 spectral curve correlates with the fluid content. Transverse relaxation encompasses three mechanisms: Surface relaxation (T_{2S}), bulk relaxation (T_{2B}), and diffusion relaxation (T_{2D}). The expression for these mechanisms is as follows:

$$\frac{1}{T_2} = \frac{1}{T_{2B}} + \frac{1}{T_{2S}} + \frac{1}{T_{2D}} = \frac{1}{T_{2B}} + \rho_2 \frac{S}{V} + \frac{D_f(\gamma G T_E)^2}{12} \quad (1)$$

where T_{2B} is the bulk relaxation time, ms; T_{2S} the surface relaxation time, ms; T_{2D} the diffusion relaxation time, ms; ρ_2 is the surface relaxation strength, μm/ms; S is the interstitial surface area, μm^2; V is the pore-throat volume, μm^3; D_f is the bulk diffusion coefficient of the pore fluid, μm^2/ms; γ is the gyromagnetic ratio, MHz/T; G is the gradient of the magnetic field, G/μm; T_E is the echo spacing time, ms.

The core holder secured the shale sample and maintained stable testing conditions, while the NMR device provided continuous monitoring of T_2 relaxation spectra, capturing fluid migration and pore saturation changes. NMR T_2 spectrum measurements were performed using an NMR core analysis device with an echo interval of 0.5 ms and a waiting time of 5,000 ms. The number of echoes was 18,000 and 32 scans were performed.

Prior to performing imbibition experiments, we calibrated the relationship between fluid saturation and signal amplitude using NMR standard porosity samples (10%, 20%, 30%, and 40%); the NMR T_2 spectral proffle of a saturated water core was tested and then the relationship between water saturation and signal amplitude of the core was calibrated.

(2) Effective pressure control system

This system controlled the confining pressure needed to simulate the effective pressure (i.e., confining pressure-pore pressure) experienced by reservoir rocks. It included a hydraulic pump capable of precise adjustments for the planned changes in effective pressure during testing.

(3) Displacement pressure control system

This system comprising a syringe pump, intermediate container, and six-way valve, was used to regulate the differential pressure and consequently the fluid injection rates and inlet pressures. The purpose of this equipment was to reproduce the pressure gradients present in shale reservoirs during hydraulic fracturing.

2.2.2 Experimental procedures

Two experimental procedures were implemented to separately investigate the influence of differential and effective pressures on the imbibition behavior.
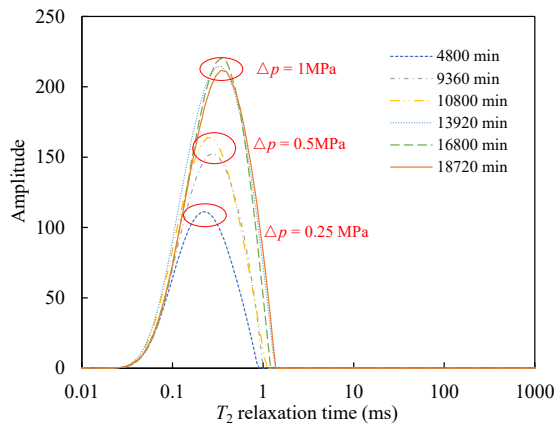
Fig. 2. S1 T_2 spectrum of imbibition under different differential pressure.
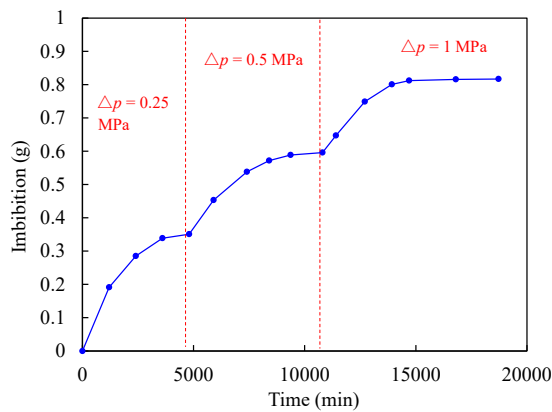
Fig. 3. Imbibition curve of S1 under different differential pressure.

Procedure I: Imbibition experiments under varying differential pressures

1) Sample preparation: Sample S1 was dried in an oven at 60 °C for 72 h to remove all residual moisture. The drying process ensured that the sample weight remained constant before testing, eliminating moisture-related variability.

2) Initial conditions: The sample was placed into the core holder. The outlet pressure was always equal at one atmospheric pressure. The effective pressure was maintained at a constant 8 MPa during the entire experiment.

3) Pressure Adjustment: The confining pressure for the first imbibition experiment was set at 8.25 MPa, with the imbibition pressure at 0.25 MPa and the outlet pressure at atmospheric pressure. When the NMR T_2 of the first imbibition remained unchanged, the confining pressure was raised to 8.5 MPa, and the inlet pressure was increased to 0.5 MPa. If the NMR T_2 of the second imbibition did not change, the confining pressure was further increased to 9 MPa, and the imbibition pressure was set to 1 MPa. When the NMR T_2 of the second imbibition remained constant, the perimeter pressure was raised to 9 MPa, and the imbibition pressure was maintained at 1 MPa.

4) Data collection: For each differential pressure, the following data were recorded at regular intervals until equi-

librium was reached:

① NMR T_2 relaxation spectra: To monitor fluid migration and distribution.

② Imbibition time: To assess the rate of fluid imbibition.

③ Imbibition mass: To measure the total volume of fluid imbibed.

5) Experiment completion: The experiment concluded after data collection for all differential pressure levels was completed.

Procedure II: Imbibition experiments under varying effective pressures

1) Sample preparation: Sample S2 underwent the same drying process as S1 to eliminate residual moisture and ensure experimental consistency. In addition, the residual rock material still available was observed using SEM after the preparation of shale Sample S2.

2) The samples were put into the core holder, and the initial outlet pressure was always atmospheric pressure. The imbibition pressure was always controlled to 0.5 MPa; the confining pressure of the first imbibition was set to 8.5 MPa, and the NMR T_2 spectral curve of the core was collected during the imbibition process, and the first imbibition experiment was stopped when the NMR T_2 spectral curve of the core did not change, and then the confining pressure was lowered to 5.5 MPa, and the effective pressure was controlled to be 5 MPa to carry out the imbibition, and the second imbibition experiment was stopped when the NMR T_2 spectral curve of the core did not change. Then reduce the perimeter pressure to 5.5 MPa, control the effective pressure to 3 MPa for imbibition, and stop the third imbibition experiment when the NMR T_2 spectrum curve of the core does not change. Finally, the pore pressure and the confining pressure of the core were unloaded, and the NMR T_2 spectrum test was performed.

3) Data collection: At each effective pressure point, the same parameters as Scheme I were recorded: NMR T_2 relaxation spectra, imbibition time.

4) Spontaneous imbibition Test: After all effective pressure tests were completed, the inlet pressure and confining pressure were fully unloaded to the atmospheric pressure, and any further immiscible displacement is caused by unconfined spontaneous imbibition. This final spontaneous imbibition process was then monitored until no further changes in T_2 spectra or imbibition mass were observed.

5) Experiment completion: This suite of experiments concluded after all pressure conditions, including those corresponding to spontaneous imbibition, were evaluated.

3. Results

3.1 Imbibition behavior under different differential pressures

The results for Scheme I, which examined the influence of the differential pressure on the imbibition behavior of Sample S1, are shown in Figs. 2 and 3.

(1) T_2 spectrum changes (Fig. 2)

The peak value of the T_2 spectrum increased progressively with increasing differential pressure, indicating a corresponding increase in the saturation of the wetting fluid. The wings of the spectrum broadened, reflecting fluid penetration into a wider range of pore sizes as differential pressure was increased. Most T_2 spectrum curves were concentrated below 1 ms, revealing that the pore network predominantly contained capillary-bound fluid and movable fluid, typical of shale formations with fine pore structures.

(2) Imbibition mass variations over time (Fig. 3)

The imbibition mass exhibited a stepwise increase as differential pressure was incrementally raised. Higher differential pressures drove greater fluid migration into the pore system, as evidenced by the gradual rise in imbibition mass with each pressure increment. At the highest differential pressure, the imbibition mass reached 0.817 g, demonstrating substantial fluid imbibition under this condition.

These findings suggest that differential pressure is a critical driver of fluid migration. Increasing the pore pressure gradient enhanced the gas-water displacement efficiency, allowing fluid to access smaller and less-connected pores, thereby improving overall imbibition efficiency.

3.2 Imbibition behavior under different effective pressures

The results for Scheme II, which investigated the effect of effective pressure on the imbibition behavior of Sample S2, are depicted in Figs. 4 and 5.

(1) T_2 spectrum changes (Fig. 4)

With decreasing effective pressure, the amplitude of the T_2 spectrum increased, revealing a growing wetting fluid saturation in the pore network. When the inlet pressure and the confining pressure were fully unloaded, it was observed that the peak value of the T_2 spectrum increased significantly as well as the maximum relaxation time, indicating improved pore connectivity and fluid mobility. A small proportion of T_2 signals with relaxation times greater than 10 ms appeared during spontaneous imbibition, accounting for 0.016% of the total spectral area, likely representing larger pores or newly formed microcracks.

(2) Imbibition mass variations over time (Fig. 5)

The imbibition mass increased in a stepwise manner as effective pressure was progressively reduced. At each effective pressure level, equilibrium was reached after a certain period, reflecting the saturation of accessible pores under the given pressure. The highest imbibition mass was achieved under spontaneous imbibition conditions, highlighting the role of effective pressure in limiting fluid accessibility during higher stress conditions.

The results demonstrate that effective pressure strongly influences imbibition behavior by altering pore accessibility and connectivity. Lower effective pressures reduce mechanical constraints on the pore structure, facilitating fluid entry into previously inaccessible pores. Under spontaneous imbibition, additional microcracks may form, further enhancing fluid migration and storage.
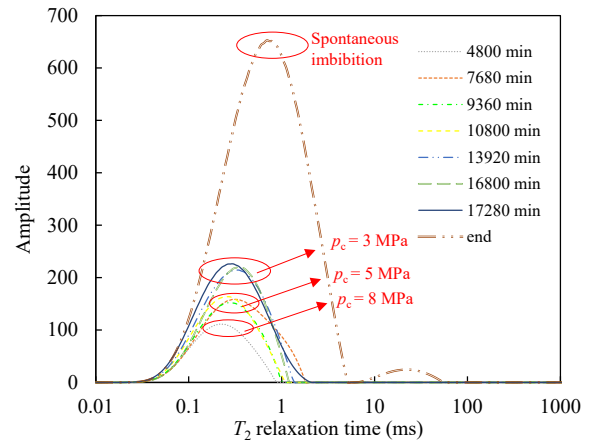
Fig. 4. S2 T_2 spectrum of imbibition under different effective pressures.
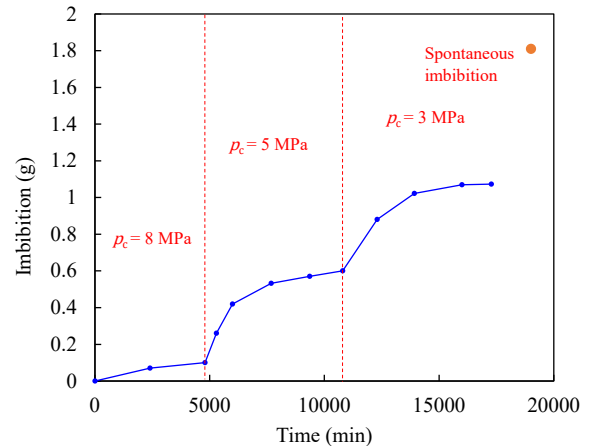
Fig. 5. Imbibition curve of S2 under different effective pressures.

4. Discussion

4.1 Influence of differential pressure

Scheme I demonstrated the critical role of differential pressure in facilitating fluid migration and improving gas-water displacement efficiency. The following key insights were derived from the experimental results.

(1) T_2 spectrum dynamics and pore filling mechanisms

The peak value of the T_2 spectrum and its maximum relaxation time are closely related to the fluid behavior in the pore structure of rocks. Specifically, when the peak value of the T_2 spectrum increases, it suggests that the pore space in the rock is more occupied by fluid, or that the pore structure becomes more connected.

The broadening of the T_2 spectrum, particularly on the left side, suggests a sequential filling mechanism, where smaller micropores are saturated first, followed by larger pores. This phenomenon indicates that differential pressure not only drives fluid migration but also redistributes flow pathways, making a broader range of pore sizes accessible for saturation. This finding underscores the significance of differential pressure in improving pore utilization.
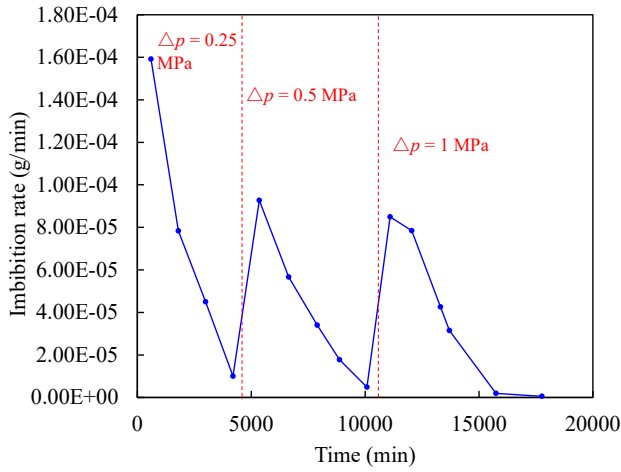
Fig. 6. Imbibition rate time curve of S1 under different displacement pressure.

Fig. 7. Curve of the moving position of the air-water interface as a function of time.

Over time, the rightward shift of the T_2 spectrum reveals the gradual progression of the gas-water interface, as gas is displaced and water progressively fills the pores. This dynamic behavior is closely tied to the magnitude of differential pressure, which governs the efficiency of gas expulsion and liquid replacement, particularly in tight pore spaces.

(2) Imbibition efficiency and kinetics

The sharp peak in imbibition rate during the early stages, followed by a gradual decline (Fig. 6), highlights the dominant role of differential pressure in overcoming initial capillary resistance. The rapid fluid influx during the initial phase can be attributed to a steep pressure gradient driving fluid migration into unoccupied pore spaces. As the pores become increasingly saturated, the imbibition rate stabilizes, reflecting the reduced pressure differential and diminishing driving force.

The experimental data revealed a stepwise increase in imbibition mass with rising differential pressure (Fig. 3). For instance, at the highest differential pressure of 1 MPa, the imbibition mass reached 0.817 g, significantly exceeding the values observed at lower pressures. This stepwise pattern highlights the critical influence of differential pressure in propagating the fluid migration front, effectively overcoming barriers and allowing water to penetrate previously isolated pore regions.

(3) Comparison with theoretical models

The comparison of imbibition results under different differential pressures showed that the imbibition replacement efficiency increased with increasing differential pressure. Assuming there are two phases, gas and water, in a single capillary tube with a radius r, the position of the interface between the two phases at time t can be expressed by Eq. (1) (Yang et al., 2023):

$$x = \frac{L}{1 - \frac{\mu_g}{\mu_w}} - \frac{\sqrt{L^2 - \frac{r^2}{4\mu_w}\left(1 - \frac{\mu_g}{\mu_w}\right)\left(\Delta p - \frac{2\sigma\cos\theta}{r}\right)t}}{1 - \frac{\mu_g}{\mu_w}}$$

(2)

where Δp represents the differential pressure (i.e., the pressure drop), MPa; σ represents the interfacial tension, mN/m; θ is
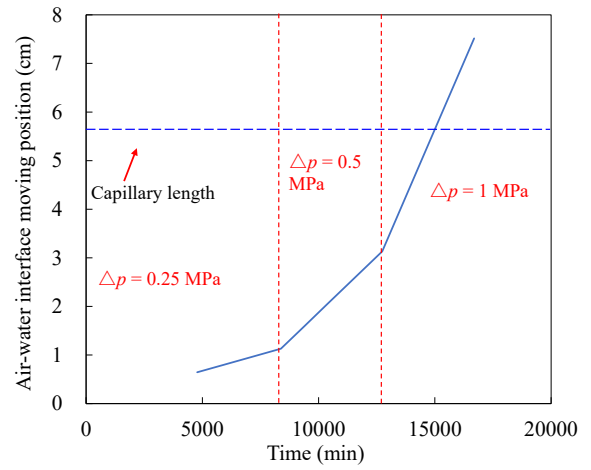
the contact angle, degree; r is the capillary tube radius, μm; μ_w and μ_g represent the viscosities of water and gas, mPa·s, respectively; L is the length of the capillary tube, μm; and x is the location of the gas-water interface, cm.

The capillary tube model (Eq. (2)) validates the experimental findings by demonstrating that higher differential pressures significantly accelerate the movement of the gas-water interface. By reducing interfacial resistance, differential pressure facilitates fluid displacement, which is consistent with an increased of the imbibition mass. This agreement with theory strengthens the connection between observed data and underlying physical processes.

As shown in Fig. 7, the gas-water interface moved toward the exit end of the capillary with increasing imbibition time. Higher differential pressure resulted in a faster advancement of the gas-water interface, as it significantly accelerates the migration process. The gas-water interface reached the exit end of the capillary at 15,000 min, which aligns with the experimental results. The presence of differential pressure ensured the advancing distance of the imbibition fluid. Without the effect of differential pressure, the scope and effectiveness of imbibition would be significantly limited.

4.2 Influence of effective pressure

Scheme II revealed the profound impact of effective pressure on pore structure, connectivity, and fluid migration behavior. Key findings from the experimental results include as follows:

(1) Pore compression and connectivity dynamics

At high effective pressures (e.g., 8 MPa), pore structures were substantially compressed, leading to restricted connectivity and suppressed fluid migration. This interpretation is consistent with the limited increase in imbibition mass and the slower imbibition rate observed in Fig. 5. The compression of smaller pores under high effective pressures significantly inhibits water penetration, reducing fluid accessibility even under forced conditions. This phenomenon highlights the mechanical constraints imposed by high effective pressures on fluid flow.
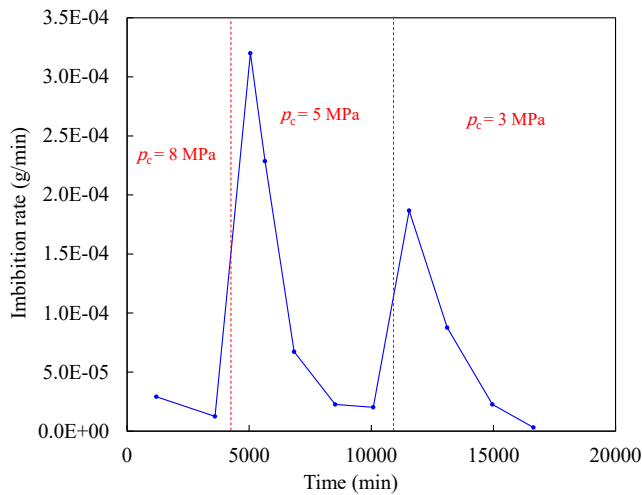
Fig. 8. Imbibition rate time curve of S2 under different effective pressure.

Fig. 9. Appearance characteristics of sample S2 before (left) and after (right) imbibition.

As effective pressure decreased to 5 and 3 MPa, the alleviation of pore compression allowed for greater fluid accessibility. The improved connectivity of the pore network facilitated more effective fluid migration, as evidenced by the steady increase in imbibition mass (Fig. 5).

As depicted in Fig. 8, when the effective pressure reached 8 MPa, the pore structure of the sample underwent significant compression, resulting in reduced pore connectivity, which notably hindered water infiltration, even under dry conditions. As the effective pressure decreased to 5 MPa, the imbibition rate initially exhibited a rapid increase but subsequently declined over time. Moreover, when the effective pressure was further lowered to 3 MPa, the water imbibition rate continued to rise with time. These experimental findings clearly demonstrate that effective pressure exerts a significant influence on the imbibition ability of the sample, suppressing the water imbibition ability of shale. In other words, a higher effective pressure correlates with a lower imbibition ability, indicating that imbibition is restrained in *in-situ* condition, which does not agree with previous results (Zhang, 2017; Li et al., 2023).

(2) Microcrack formation

In the presence of effective stress, the area enclosed by the NMR T_2 spectral curve gradually increased as effective pressure decreased. When the effective pressure was reduced from 8 to 5 MPa, the NMR T_2 spectrum area expanded by 55.99%. Similarly, when the effective pressure decreased from 5 to 3 MPa, the NMR T_2 spectrum area increased by 52.74%. However, when all pressures were released, the T_2 spectrum expanded significantly. The NMR T_2 spectral area expanded by 256.67%, and a distinct double-peak feature was observed (Fig. 4). This indicates that the release of pressure led to a substantial increase in water absorption within the larger pores, and the emergence of a new peak in the T_2 spectrum appears to be related to the formation of microcracks observed in the photos of our samples (Fig. 9) and SEM images (Fig. 10). Through SEM observations and sample photographs, it was found that the cracks in the samples were relatively few and fine before imbibition; however, the number of cracks increased, and the width and depth of some cracks became significantly larger after imbibition. The results of this experiment indicate that imbibition contributes to the formation of microcracks in the rock samples, a conclusion that aligns with the findings of previous researchers (Zhou et al., 2024). However, it is important to note that the presence of effective pressure significantly inhibited the formation of microcracks in the rock samples.

It was widely accepted that the occurrence of microcracks is primarily induced by the hydration and swelling of clay. However, under conditions of confining pressure, no significant cracks formed, indicating that confining pressure exerts an inhibitory effect on crack generation. When clay undergoes hydration and swelling, it absorbed water molecules, resulting in an increase in volume. In an environment without confining pressure, the direction of clay expansion was relatively unrestricted, and local stress concentrations might exceed the tensile strength of the rock, thereby triggering the formation of microcracks. Conversely, in the presence of confining pressure, the expansion of clay was subject to mandatory constraints and was confined within the rock. In this scenario, the pressure generated by the expansion must overcome the confining pressure to induce effective deformation of the rock, thus inhibiting the formation of cracks.

4.3 Comparative analysis: Differential vs. effective pressure

(1) Unique contributions to imbibition efficiency

Differential pressure acts as the primary driving force for fluid migration by creating a pressure gradient that overcomes capillary forces, thereby accelerating gas-water displacement and enhancing imbibition efficiency (as discussed in Section 4.1). However, the effectiveness of differential pressure is constrained by the connectivity and accessibility of the pore network. Under high effective pressure conditions, mechanical compression of the pores reduces connectivity, limiting the ability of differential pressure to fully drive fluid migration (Fig. 6).

Effective pressure, on the other hand, directly controls the structural characteristics of the pore network, including pore compression, connectivity, and permeability (as discussed in Section 4.2). When effective pressure is decreased, the forma-
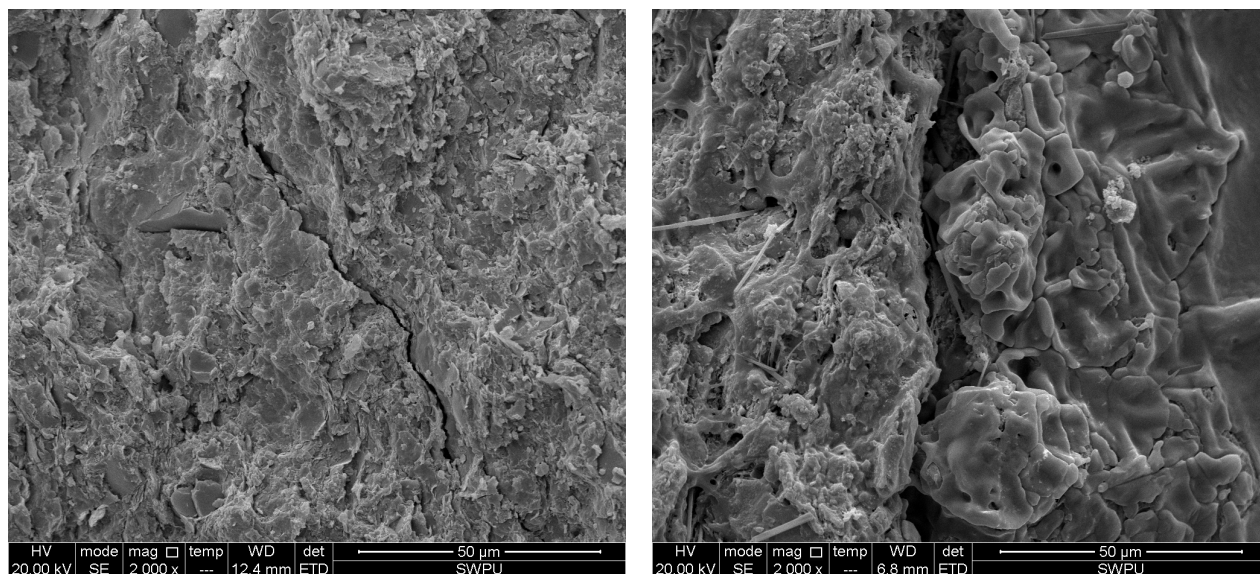
Fig. 10. SEM results before (left) and after spontaneous imbibition (right) of S2.

tion of microcracks and the expansion of the pore network significantly improve fluid accessibility, creating conditions that amplify the efficiency of differential pressure.

(2) Interdependence of differential and effective pressures

At low effective pressures, especially no effective pressure, the pore network's improved connectivity facilitates fluid migration into previously inaccessible regions (Fig. 5). This enhanced connectivity allows differential pressure to fully exert its driving force, enabling deeper and more extensive fluid migration. The synergistic effect lies in the interaction between reduced mechanical constraints and increased pressure gradients, which together drive fluid into tight and low-connectivity zones.

The synergy between differential and effective pressures extends beyond individual pores. By connecting isolated pore spaces through microcracks, reduced effective pressure enables differential pressure to drive gas-water displacement across a broader pore network. This combined effect enhances not only the localized imbibition process but also the overall connectivity and permeability of the reservoir, making it particularly beneficial for low-permeability formations.

5. Conclusions

1) During the imbibition process under different differential pressures, micropores were filled firstly, followed by larger pores as the differential pressure increased. Higher differential pressure was beneficial for improving the gas-water imbibition replacement efficiency during the soaking process of shale gas.

2) At constant differential pressure, the imbibition replacement efficiency increased as the effective pressure decreased. When the effective pressure was completely unloaded, the feature of the T_2 spectrum curve behaved from single-peak to double-peak, new microcrack was formed, and a significant increase in imbibition replace-

ment efficiency.

3) Differential pressure and effective pressure are two critical factors controlling shale imbibition. Therefore, the influence of pressure conditions on shale imbibition should be given greater attention in future research and practical applications.

Acknowledgements

Conflict of interest

The authors declare no competing interest.

References

Akbarabadi, M., Piri, M. Nanotomography of the spontaneous imbibition in shale. Paper URTEC 1922555 Presented at the SPE/AAPG/SEG Unconventional Resources Technology Conference, Denver, Colorado, USA, 25-27 August, 2014.

Ali, M., Ali, S., Mathur, A., et al. Organic shale spontaneous imbibition and monitoring with NMR to evaluate *in-situ* saturations, wettability and molecular sieving. Paper URTEC-2020-3096 presented at the SPE/AAPG/SEG Unconventional Resources Technology Conference, Virtual, 20-22 July, 2020.

Cai, J., Perfect, E., Cheng, C., et al. Generalized modeling of spontaneous imbibition based on Hagen-Poiseuille flow in tortuous capillaries with variably shaped apertures. Langmuir, 2014, 30(18): 5142-5151.

Cheng, H., Zhang, J., Leng, R., et al. Mechanism of imbibition in shale pores based on imbibition nuclear magnetic experiment and LBM method. Chemistry and Technology of Fuels and Oils, 2021, 57(5): 387-395.

Chen, Z., Ning, Z., Yu, X., et al. New insights into spontaneous imbibition in tight oil sandstones with NMR. Journal of Petroleum Science and Engineering, 2019, 179(1): 455-464.

Ding, Y., Yu, X., Liu, X., et al. Novel analytical model of shale spontaneous imbibition considering the hydration effect. Energy & Fuels, 2021, 35(22): 18518-18532.

Dou, Z., Yang, Z., Dong, C., et al. Rock physical evolution and microscopic flow mechanism of massive energy replenishment in tight oil reservoirs. Advances in Geo-Energy Research, 2024, 14(1): 49-63.

Du, M., Yang, Z., Lv, W., et al. Experimental study on microscopic production characteristics and influencing factors during dynamic imbibition of shale reservoir with online NMR and fractal theory. Energy, 2024, 310(12): 133244.

Gao, H., Li, H. Determination of movable fluid percentage and movable fluid porosity in ultra-low permeability sandstone using nuclear magnetic resonance (NMR) technique. Journal of Petroleum Science and Engineering, 2015, 133: 258-267.

Hughes, J. A reality check on the shale revolution. Nature, 2013, 494(7437): 307-308.

Kerschke, D. I., Schulz, H. M. The shale gas potential of Tournaisian, Visean, and Namurian black shales in North Germany: baseline parameters in a geological context. Environmental Earth Sciences. 2013, 70: 3817-3837.

Lai, D., Li, Z., Wei, Q., et al. Experimental investigation of spontaneous imbibition in a tight reservoir with nuclear magnetic resonance testing. Energy & Fuels, 2016, 30(11): 8932-8940.

Liu, Y.,Yao Y.,Liu, D., et al. Shale pore size classification: An NMR fluid typing method. Marine and Petroleum Geology, 2018, 96: 591-601.

Li, Y., Li, M., Li, H., et al. Investigation of shale imbibition capability and the influencing factors based on a convenient method. Arabian Journal of Geosciences, 2023, 16: 65.

Li, Y., Yuan, J., Wang, Z, et al. Modeling of magnetic fields for application in nuclear magnetic resonance gyroscopes. Paper MIC.2013.6757911 Presented at the IEEE 2013 2nd International Conference on Measurement, Information and Control, Harbin, China, 16-18 August, 2013.

Lu, H., Xu, Y., Duan, C., et al. Experimental study on capillary imbibition of shale oil in nanochannels. Energy & Fuels, 2022, 36(10): 5267-5275.

Makhanov, K., Dehghanpour, H., Kuru, E. An experimental study of spontaneous imbibition in Horn River shales. Paper SPE 162650 Presented at the SPE Canadian Unconventional Resources Conference, Calgary, Alberta, Canada, 30 October-1 November, 2012.

Pan, B., Clarkson, C. R., Younis, A., et al. New methods to evaluate impacts of osmotic pressure and surfactant on fracturing fluid loss and effect of contact angle on spontaneous imbibition data scaling in unconventional reservoirs. Fuel, 2022, 328: 125328.

Rezaveisi, M., Ayatollahi, S., Rostami, B. Experimental investigation of matrix wettability effects on water imbibition in fractured artificial porous media. Journal of Petroleum Science and Engineering, 2012, 86-87: 165-171.

Roychaudhuri, B., Tsotsis, T. T., Jessen, K. An experimental investigation of spontaneous imbibition in gas shales. Journal of Petroleum Science and Engineering, 2013, 111: 87-97.

Saidzade, A., Liu, N., Mokhtari, M., et al. Spontaneous imbibition in shales under one-end-open boundary condition: Effect of wettability, porosity, and bedding orientation. Paper URTEC 2020-3168 Presented at the SPE/AAPG/SEG Unconventional Resources Technology Conference, Virtual, 20-22 July, 2020.

Siddiqui, M. A. Q., Chen, X., Iglauer, S., et al. A Multiscale study on shale wettability: Spontaneous imbibition versus contact angle. Water Resources Research, 2019, 55(6): 5012-5032.

Sun, B., Yang, E., Wang, H., et al. Using NMR to characterize fluids in tight rock unconventional and shale formations. Paper SPWLA-2016-PP presented at the SPWLA 57$^{/rmth}$ Annual Logging Symposium, Reykjavik, Iceland, 26 June, 2016.

Sun, Y., Li, Q., Chang, C., et al. NMR-based shale core imbibition performance study. Energies, 2022, 15(17): 6319.

Su, Y., Sun, Q,. Wang, W., et al. Spontaneous imbibition characteristics of shale oil reservoir under the influence of osmosis. International Journal of Coal Science & Technology, 2022, 9(1): 69.

Tang, J., Wu, H., Cheng, Q., et al. Experimental investigation on the spontaneous imbibition characteristics of shale under the combined action of CO_2 and Water. Energy & Fuels, 2024, 38(5): 3871-3879.

Testamanti, M. N., Rezaee, R. Determination of NMR T_2 cut-off for clay bound water in shales: A case study of Caryginia Formation, Perth Basin, Western Australia. Journal of Petroleum Science and Engineering, 2017, 147: 497-503.

Wang, C., Gao, H., Gao, Y., et al. Influence of pressure on spontaneous imbibition in tight sandstone reservoirs. Energy & Fuels, 2020, 34(8): 9275-9282.

Wang, L., Yu, F., Shi, J., et al. Study on engineering geological characteristics of southwest shale oil based on nuclear magnetic resonance imbibition flooding technology. Acta Geophysica, 2024, 72(5): 3309-3323.

Wang, M., Jiang, L., Bao, J., et al. Imbibition experimental description and methods' applicability evaluation. Petrochemical Application, 2015, 34(12): 4. (in Chinese)

Wei, J., Fu, L., Zhao, G., at al. Nuclear magnetic resonance study on imbibition and stress sensitivity of lamellar shale oil reservoir. Energy, 2023, 282: 128872.

Wei, J., Shang, D., Zhao, X., et al. Experimental study on production characteristics and enhanced oil recovery during imbibition and huff-n-puff injection in shale reservoir. Capillarity, 2024, 12(2): 41-56.

Xiao, W., Yang, Y., Li, M., et al. Experimental study on the oil production characteristics during the waterflooding of different types of reservoirs in Ordos Basin, NW China. Petroleum Exploration and Development, 2021, 48(4): 935-945.

Yang, L., Dou, N., Lu, X., et al. Advances in understanding imbibition characteristics of shale using an NMR technique: A comparative study of marine and continental shale. Journal of Geophysics and Engineering, 2018, 15(4): 1363-1375.

Yang, Y., Xiao, W., Zheng, L., et al. Pore throat structure heterogeneity and its effect on gas-phase seepage capacity in tight sandstone reservoirs: A case study from the Triassic Yanchang Formation, Ordos Basin. Petroleum Science, 2023, 20(5): 2892-2907.

You, L., Xu, J., Kang, Y., et al. Water adsorbed by organic rich shale considering oxidation. Journal of Southwest Petroleum University, 2019, 41(26): 106-116. (in Chinese)

Yu, H., Xu., W., Li, B., et al. Hydraulic fracturing and enhanced recovery in shale reservoirs: Theoretical analysis to engineering applications. Energy & Fuels, 2023, 37(14): 9956-9997.

Yuan, Y., Reza, R., Zhou, M., et al. A comprehensive review on shale studies with emphasis on nuclear magnetic resonance (NMR) technique. Gas Science and Engineering, 2023, 120(4): 205163.

Zhang, H. Experiment research on behavior of spontaneous imbibition in shale reservoirs. Chengdu, Southwest Petroleum University, 2017. (in Chinese)

Zhao, Z., He, Y., Guo, J., et al. Experimental study on the forcible imbibition law of water in shale gas reservoirs. Processes, 2023, 11(4): 1057.

Zhou, C., He, Z., Qin, X., et al. Experimental research on imbibition law of Jurassic continental shale in Fuxing area. Petroleum Geology and Recovery Efficiency, 2024, 31(6): 118-126. (in Chinese)